Heliyon 10 (2024) e35428

Contents lists available at ScienceDirect

Heliyon

journal homepage: www.cell.com/heliyon

Research article

Comparative analysis of the mutational landscape and evolutionary patterns of pancreatic ductal adenocarcinoma metastases in the liver or peritoneum

Guoliang Yao [a,1], Yanfeng Zhu [b,1], Chunhui Liu [a], Yanwen Man [a], Kefeng Liu [a], Qin Zhang [c], Yuan Tan [c], Qianqian Duan [c], Dongsheng Chen [c], Zunguo Du [d,*,1], Yonggang Fan [a,**,1]

[a] Department of General Surgery, The First Affiliated Hospital of Henan University of Science and Technology, 636 Guanlin Road, Luoyang, China
[b] Department of Nursing, Huashan Hospital, Fudan University, No.12 Middle Urumqi Road, Shangha, China
[c] Jiangsu Simcere Diagnostics Co., Ltd., Nanjing Simcere Medical Laboratory Science Co., Ltd., The State Key Laboratory of Neurology and Oncology Drug Development, China
[d] Department of Pathology, Huashan Hospital, Fudan University, No.12 Middle Urumqi Road, Shanghai, China

ARTICLE INFO

Keywords:
Liver metastasis
Peritoneum metastasis
Whole exome sequencing
Mutation
Clone evolution

ABSTRACT

Background: Pancreatic ductal adenocarcinoma (PDAC) often presents with liver or peritoneal metastases at diagnosis. Despite similar treatment approaches, patient outcomes vary between these metastatic sites. To improve targeted therapies for metastatic PDAC, a comprehensive analysis of the genetic profiles and evolutionary patterns at these distinct metastatic locations is essential.

Methods: We performed whole exome sequencing on 44 tissue samples from 27 PDAC patients, including primary tumours and matched liver or peritoneal metastases. We analysed somatic mutation profiles, signatures, and affected pathways for each group, and examined clonal evolution using subclonal architectures and phylogenetic trees.

Results: KRAS mutations remained the predominant driver alteration, with a prevalence of 89 % across all tumours. Notably, we observed site-specific differences in mutation frequencies, with *KRAS* alterations detected in 77.8 % (7/9) of peritoneal metastases and 87.5 % (7/8) of liver metastases. *TP53* mutations exhibited a similar pattern, occurring in 55.6 % (5/9) of peritoneal and 37.5 % (3/8) of liver metastases. Intriguingly, we identified site-specific alterations in DNA repair pathway genes, including *ATM* and *BRCA1*, with distinct mutational profiles in liver versus peritoneal metastases. Furthermore, liver metastases demonstrated a significantly higher tumor mutational burden (TMB) compared to peritoneal metastases (median [IQR]: 2.14 [1.77–2.71] vs. 1.29 [1.21–1.69] mutations/Mb; P = 0.048).

Conclusions: In conclusion, metastasis of pancreatic cancer may be influenced by variables other than *KRAS* mutations, such as *TP53*. PDAC peritoneal and liver metastases may differ in potential therapeutic biomarkers. Further inquiry is needed on the biological mechanisms underlying metastasis and the treatment of diverse metastases.

* Corresponding author. Department of Pathology, Huashan Hospital, Fudan University, No.12 Middle Urumqi Road, Shanghai, China.
** Corresponding author.
E-mail addresses: duzunguo@fudan.edu.cn (Z. Du), fanyonggangdoc@163.com (Y. Fan).
[1] Contributed to this work equally.

https://doi.org/10.1016/j.heliyon.2024.e35428
Received 19 February 2024; Received in revised form 2 July 2024; Accepted 29 July 2024
Available online 30 July 2024

Implications for practice

Over 50 % of pancreatic ductal adenocarcinoma (PDAC) patients have liver and peritoneal metastases at diagnosis. Metastasis treatment regimens are similar, but patient outcomes vary. We compared the mutation landscape and clone evolution of PDAC patients with liver and peritoneum metastasis or non-metastatic. Our findings will offer fresh insights into the biology of the metastatic process in PDAC, as well as implications for novel therapeutic approaches to precisely manage distinct distant metastases.

1. Introduction

Pancreatic ductal adenocarcinoma (PDAC) is one of the most aggressive and fatal cancers in the world [1]. Approximately fifty percent of newly diagnosed PDAC patients have distant metastases [2]. The peritoneum is the second most common site of metastasis after the liver [3,4]. Peritoneal metastases are present in 50 % of patients with pancreatic cancer at the time of death, but treatment of these dismal metastases remains a clinical challenge [5]. Surgery is the only currently curative treatment for pancreatic cancer. However, once distant metastases are diagnosed, the National Comprehensive Cancer Network (NCCN) Clinical Practice Guidelines do not recommend radical surgery, resulting in an extremely low 5-year survival rate (1 %) and a median survival time of approximately 5.4–8.2 months [6]. Metastasis is a complicated process with many steps, including invasion, intravasation, survival in the bloodstream, extravasation, adaptation to survival in a new microenvironment, colonisation, and outgrowth at a different body site [7]. Recent studies that compared primary tumours and metastases suggest that different types of cancer may have different metastatic progression patterns. However, it is still not known whether metastasis to different organ sites follows the same or a different progression paradigm in cancer [8]. A better comprehension of these issues will not only yield new insights into the biology of metastatic processes but may also disclose differences in the therapeutic strategies that concurrently target primary and metastatic malignancies.

Herein, for the first time, we systematically investigated the genomic profiles of synchronous resected primary tumours (PTs), paired liver metastases (Li-M), and peritoneum metastasis (Pe-M) from 27 treatment-naïve PDACs carrying hepatic or peritoneum metastases. We sought to unravel the underlying mechanism of PDAC metastasis, which would shed light on the development of novel therapeutic strategies for metastatic PDAC patients through whole exome sequencing.

2. Materials and methods

2.1. Sample collection

Primary surgically resected PDAC-matched metastatic sites (liver or peritoneum) were collected between June. 2020 and August. 2022 in the First Affiliated Hospital of Henan University of Science and Technology. Yet, six samples were removed from quality control due to tumour purity. Whole exome sequencing (WES) was also performed on three main or metastatic foci. Two expert pathologists assessed histologic kinds and cancer cell proportions on H&E-stained slides. Each sample must have at least 50 % tumour nuclei and less than 20 % necrosis on histology to be sequenced [9]. The ethics committees of the First Affiliated Hospital of Henan University of Science and Technology approved the study, and informed consent was obtained before sample collection. The study was conducted in accordance with the Declaration of Helsinki.

2.2. DNA extraction and library construction

Genomic DNA (gDNA) of formalin-fixed and paraffin-embedded (FFPE) tissues was extracted using the Genomic DNA Tissue Extraction Kit (Concert®). DNA samples were quantified with the Qubit dsDNA HS Assay kit (Life Technologies, Carlsbad, CA) per the manufacturer's recommended protocol.

2.3. Whole exome sequencing

NGS tests targeting the Whole exome Hyb Panel were performed at Simceredx company (Nanjing, China) following the manufacturer's instructions. In brief, 200 ng gDNA was sheared into 200–300 bp with a combined bisulfite restriction assay. Indexed paired-end adaptors for the Illumina platform were synthesized by Integrated DNA Technologies (IDT). End repair, A-tailing and adaptor ligation of sheared DNA were performed with reagents from the KAPA Hyper DNA Library Prep kit (Roche Diagnostics). Unligated adaptors were removed by the size selection function of Agencourt AMPure XP beads (Beckman Coulter), and the ligation products were PCR amplified to form a prelibrary for hybridization. Prepared DNA libraries were sequenced on an Illumina NovaSeq6000 platform (Illumina, San Diego, CA), and 150 bp paired-end reads were generated. The principle of sequencing was sequencing by synthesis, and the mean sequencing depth of tissue was 500X.

2.4. Data filtering and variant calling

The sequencing reads were parsed with fastp (V.2.20.0) for adapter pruning, and low-quality bases were removed [10]. Using Burrows–Wheeler Aligner version 0.7.17 (http://bio-bwa.sourceforge.net/index.shtml), cleaned paired-end reads were aligned to the hg19 human genome reference [11]. Using Picard (https://broadinstitute.github.io/picard/), duplicate reads were then removed from

the aligned and sorted Binary Alignment Map files (Broad Institute, Cambridge, MA). MuTect2 (v 4.2.3) from GATK (Broad Institute) was utilized to detect SNVs and minor indels [12]. Subsequently, the variant call format (VCF) was annotated with ANNOVAR [13]. An SNV was considered a true positive if the variant allele frequency (VAF) was greater than 1 % and the read depth was greater than 200X. Variants were labelled germline if they were present in any of the following four germline population variant databases (PVDs) at a minor allele frequency (MAF) of 0.1 %: 1000 Genomes phase 3 (https://www.internationalgenome.org/data),ESP6500 (http://evs.gs.washington.edu/EVS), gnomAD (v2.1.1, https://gnomad.broadinstitute.org/) or dbSNP build141 (GRCh37.p13, https://www.ncbi.nlm.nih.gov/snp/). Variants not found in any of the PVDs at the 0.1 % MAF threshold were labelled somatic. Additionally, variants were labelled somatic if they were found in COSMIC database release version 85, with two or more occurrences, even if they were also found in a germline population database. Finally, variants were labelled germline if they were present as a benign or likely benign variant in either ClinVar (https://www.ncbi.nlm.nih.gov/clinvar) or InterVar (http://wintervar.wglab.org/). Additional analysis of the mutation filter and inspection was implemented by custom scripts. All mutations in coding regions were manually checked using the Integrative Genomics Viewer (version (v2.14.1, https://igv.org/) [14]. DNA CNVs were detected by using Detection of Exon Copy Number variants (DECoN, https://github.com/RahmanTeam/DECoN) [15]. We surveyed the discordance of the CNV profile between paired primary and metastatic tumours using Pearson correlation analysis.

2.5. Jaccard similarity index

We used the Jaccard similarity index (JSI) to quantify mutational similarity between primary and metastasis pairs [16]. The number of metastasis-private, primary-private and primary-metastasis shared SNVs for each P/M pair was denoted L_m, L_p and W_s, respectively. For two sets, the Jaccard similarity index (JSI) is defined for the intersection divided by the union of these two sets. Thus, the JSI for a P/M pair can be defined as:

$$\mathrm{JSI} = \frac{Ws}{Lm + Lp + Ws}$$

2.6. Mutational signature analysis

Nonsynonymous somatic SNVs were analysed to define mutational signatures, including six categories of base substitutions, namely, T > A, T > C, T > G, C > A, C > G, and C > T, in each included sample. We extracted the potential mutational signatures by using nonnegative matrix factorization (R package maftools, v 2.6.05) [17]. We then analysed and compared the relative contribution of different signatures in the primary lesions of patients with those in Li-M and Pe-M. We also used nonnegative matrix factorization (NMF) to predict signatures and compared the identified signatures with the 30 known signatures in the Catalogue of Somatic Mutations in Cancer (COSMIC, https://cancer.sanger.ac.uk/cosmic/signatures_v2).

2.7. Classification of driver mutations

We collated a driver gene list using genes identified in the COSMIC cancer gene census (v.85) [18], supplemented with those identified in large-scale pancancer analyses [19] and previous large-scale sequencing landscape studies across 12 major cancer types [20,21]. Any nonsynonymous variant located within one of these genes underwent further categorization based on the following criteria. If the mutation was found to be deleterious (either a stop-gain or predicted deleterious in three out of the five computational approaches applied: Sift, SIFT4G, Polyphen2, FATHMM and MutationTaster) and the gene was annotated as being recessive by COSMIC (tumour suppressor) [22–26], the variant was classified as a driver mutation. We collected actionable unique alterations in each liver or peritoneum metastatic group of PDAC and cross-referenced them with the OncoKB (https://www.oncokb.org/) and COSMIC (https://cancer.sanger.ac.uk/actionability) databases to identify potential drug targets and therapeutic strategies.

2.8. Clonality analysis

The clonal and subclonal architecture of paired primary with metastasis focal were estimated using the R package SciClone [27]. For each tumour, variants belonging to the cluster with the highest VAF were annotated as ‘‘clonal’’, whereas those belonging to clusters with a lower VAF were annotated as ‘‘subclonal’’. The R package ClonEvol (v0.99.11) [28] was utilized to reconstruct the cellular fraction of the clones, as well as to probabilistically model the clonal ordering constraints and provide visualization for each patient. The tumour clonal evolution of each patient was visualized using the R package fishplot (version 0.2) [29].

2.9. Phylogenetic Analysis

To illustrate the clonal architecture of each paired patient, we constructed phylogenetic trees using somatic mutations. The clonal and subclonal architecture of paired primary with metastasis focal were estimated using the R package SciClone [27], which implements a Bayesian inference model to assign SNVs to clonality clusters based on VAF. Clonal architecture was inferred from copy number neutral (diploid) genomic regions, and only somatic variants supported by at least 100 reads were considered for the analyses. For each tumour, variants belonging to the cluster with the highest VAF were annotated as ‘‘clonal’’, whereas those belonging to clusters with a lower VAF were annotated as ‘‘subclonal’’. The R package ClonEvol (v0.99.11) [28] was utilized to reconstruct the

cellular fraction of the clones, as well as to probabilistically model the clonal ordering constraints and provide visualization for each patient. The number of bootstraps was set as 1000. The minimum probability that a VAF estimate for a clone in a sample is nonnegative in an accepted clonal ordering was set as 0.01. The cluster centre used the median of each cluster. The tumour clonal evolution of each patient was visualized using the R package fishplot (version 0.2). The length of the trunk and branch represented the number of shared and specific mutations, respectively. The branch lengths were estimated through ancestral state reconstruction with the accelerated transformation method [30]. The candidate driver mutations were mapped to the trunk and branches of each phylogenetic tree to depict the molecular processes. iTOL (v6.7.5) was used to draw evolutionary trees [31].

2.10. Pathway enrichment analysis

For each sample group, the altered genes were evaluated for their potential enrichment in the Kyoto Encyclopedia of Genes and Genomes (KEGG) pathways (https://www.kegg.jp and KEGG.db package version 3.2.3) using gene set overrepresentation analysis on the basis of Fisher's exact test, which was implemented in the R package clusterProfiler (version 3.6.0) [32].

2.11. Statistical analysis

All tests were performed with the R environment version 4.0.2 (R core team, Vienna, Austria) or GraphPad Prism 6.0 (GraphPad Software, San Diego, CA). Comparisons between paired primary tumours and metastases were based on Student's *t*-test. The nonparametric Wilcoxon rank-sum test was applied for comparison of mutation counts and branch lengths. If not noted otherwise, the tests applied were two-sided. As per the convention, p values less than 0.05 were considered statistically significant.

3. Results

3.1. Clinical and sample information

We performed WES sequencing on 44 samples taken from 27 treatment-naïve patients with PDAC (17 males, 10 females). The samples analysed in this study, no metastasis occurred within the first year after surgery (non-PTs), paired liver-metastatic primary lesions (LiM-PTs) and liver metastatic lesions (LiM-MTs), and paired samples of peritoneal-metastatic primary lesions (PeM-PTs) and peritoneal metastatic lesions (PeM-MTs). The patient flow is illustrated in Fig. 1. The mean age of these patients was 63 (range: 38–81). Supplementary Table S1 and Fig. S1 provide the clinicopathological characteristics of all enrolled patients.

3.2. The mutation landscape of the pancreatic cancer cohort and similarity analysis of the paired LiM-PTs/MTs and PeM-PTs/MTs

To decipher the mutation landscape difference in separate groups, we performed WES sequencing on 44 samples. The WES results of all 44 samples showed that the *KRAS* mutation was the most common mutation in pancreatic cancer, with a mutation frequency of 89 %. This was followed by *TP53, GOLGA8J, TTN, and SMAD4,* and the mutation frequencies were 50 %, 25 % and 25 %, 23 %, respectively (Fig. 2A). The incidence of *KRAS* mutations in different types of primary sites, including LiM-PTs, PeM-PTs, and non-PTs, was 90 % (9/10), 90 % (9/10), and 88.9 % (8/9), respectively (Fig. 2B). The mutation frequencies of all genes in primary tumours are shown in Supplementary Table S2. It is noteworthy that modifications of *PCDHB14* and *PXDN* were solely identified in the non-PT group with mutation frequencies of 40.0 % and 30.0 %, respectively. *MUC16* was mutated only in LiM-PTs with a mutation

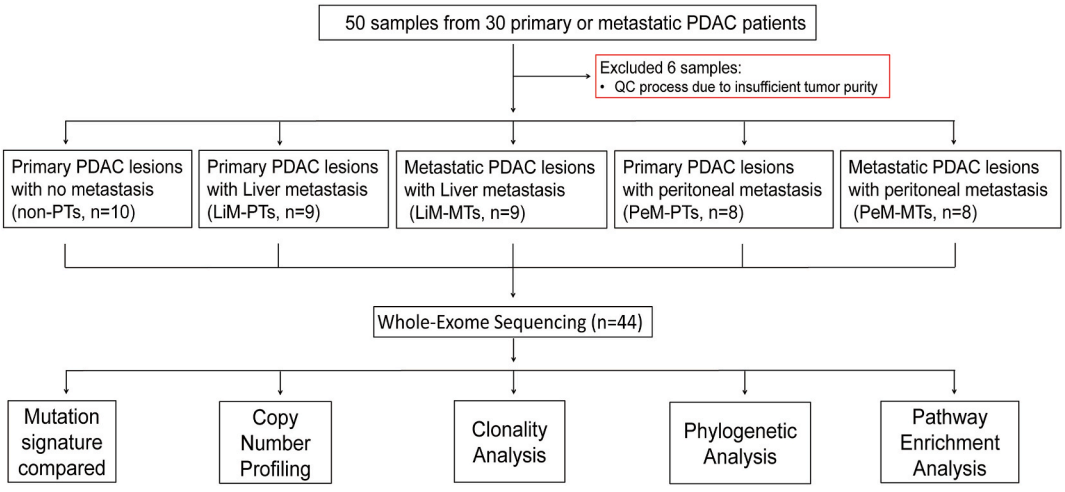

Fig. 1. Patient flow.

frequency of 33.3 %. *ZNF594* was mutated only in PeM-PTs, with a mutation frequency of 30 % (Fig. 2B–Supplementary Table S2). Mutations were also found in liver and peritoneal metastases. Cross-referencing with the OncoKB and COSMIC databases reveals unique mutations that may benefit patients from targeted therapy. In contrast to liver metastasis, peritoneal metastasis has mutations in DNA repair pathway genes such as *ATM* and *BRAC1* (Table 1). The results indicated that treating hepatic and peritoneal metastases in pancreatic cancer may require different therapeutic approaches. Next, we examined shared and private mutations in paired liver and peritoneal metastasis samples. As shown in Fig. 2C, there was considerable variation in mutations among individual patients within each group. The proportion of shared mutations between each primary lesion and its corresponding paired samples was calculated. The median value of shared mutations in the liver metastasis group was 33.13 % (range: 8.57%–72.26 %), while that in the peritoneal metastasis group was 42.12 % (range: 6.26%–66.19 %) (Supplementary Table S3). We also computed the Jaccard similarity index (JSI), an indicator of mutational resemblance, and found no discernible difference in JSI between the two groups ($p = 0.81$, Fig. 2D). The JSI of each paired sample also showed the same trend as the shared mutation ratio, that is, large individual differences (Figs. 2E–1F). Furthermore, the LiM-MT group exhibited a higher TMB than the PeM-MT group (LiM-MT: 2.14(1.77–2.71) vs PeM-MT: 1.29(1.21–1.69), $p = 0.048$, Fig. 2G). However, there was no statistically significant difference between paired primary and corresponding metastases (LiM-PTs vs. LiM-MTs: 2.09(1.32–2.63) vs:2.14(1.77–2.71), $p = 0.49$; PeM-PTs vs. PeM-MTs: 1.72(1.39–2.08) vs 1.29(1.21–1.69), $p = 0.38$, Fig. 2G).

3.3. The mutation signature of the pancreatic cancer cohort

To infer the underlying mutational processes, we delineated the mutational signatures based on somatic mutation data. The mutation types of all samples are shown in Fig. 3A–C. Single nucleotide polymorphisms (SNPs) were the predominant type of mutation, with missense mutations accounting for the vast majority (Fig. 3A). In terms of mutation patterns, the most prevalent base change observed in the samples was C > T (Fig. 3B). The median number of variants per sample was 54 (Fig. 3C). The mutation types of the highly recurrent genes are illustrated in Fig. 3D. Both the LiM and PeM groups exhibited a significantly higher proportion of C > T and transitions (Ti)/transversions (Tv), as shown in Fig. 3E–F. According to the cosine similarity, in the LiM-MT group, the 3 mutational

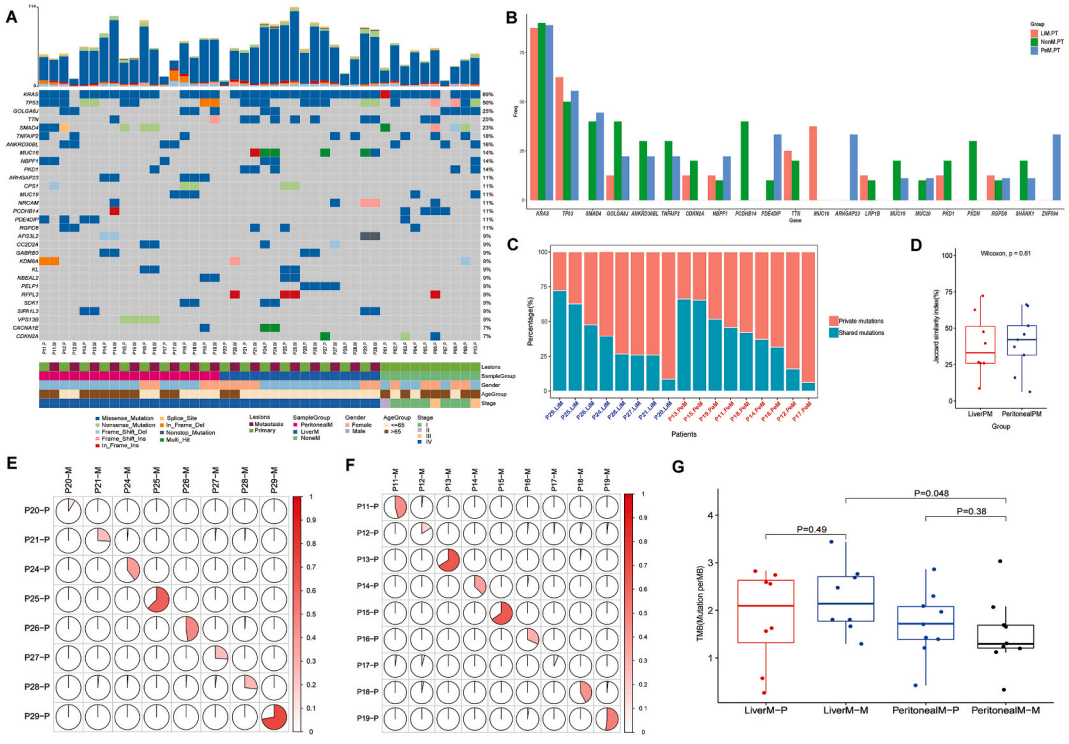

Fig. 2. A. Mutation landscape of all samples. The top panel represents the number of somatic mutations in each sample. The middle panel represents the matrix of mutations in a selection of frequently mutated genes. Columns represent samples. Three clinicopathological characteristics (sex, stage, and smoking history) are presented below; B. Bar plot of the top recurrent mutation frequency in the primary loci of different groups (LiM-PT, PeM-PT, and non-PT groups). C. The percentages of identified somatic mutations that were found to be shared (present in both primary and metastatic lesions) or private (present only in primary or metastatic lesions) in each tumor specimen D. Statistical analysis of the Jaccard similarity index in the LiM and PeM groups. E-F. The somatic mutation consistency of paired primary and metastasis samples in the LiM group (E) and in the PeM group (F); G. Statistical analysis of TMB in primary-metastasis paired sample groups.

Note: P11.P and P11.M refer to the primary and metastasis lesion of patient 11 (A); P20–P and P20-M refer to the primary and metastasis lesion of patient 20 (E); LiverM-P and Liver-M represent the primary and liver metastasis lesion of the PDAC liver metastasis group (G).

Table 1
The unique actionable gene mutation of Liver or Peritoneal metastic foci refer to OncoKB and COSMIC database.

Gene	Mutation Type	Mutation Group	Potential Target Drug or Treatment
ARID1A	Truncating Mutations	Uniq mutation in Liver metastasis	Tazemetostat; PLX2853
TNFRSF8	Oncogenic SNV Mutations	Uniq mutation in Liver metastasis	Brentuximab vedotin + Cyclophosphamide + Doxorubicin hydrochloride + Prednisone
ERBB3	Oncogenic Mutations	Uniq mutation in Liver metastasis	Chemotherapy + Pertuzumab
KDR	Oncogenic Mutations	Uniq mutation in Liver metastasis	Dovitinib; Sunitinib; Erlotinib + Sunitinib
TET2	Oncogenic Mutations	Uniq mutation in Liver metastasis	Azacitidine + Lenalidomide; Cytarabine + Daunorubicin + Glasdegib; Azacitidine; Azacitidine + Lenalidomide
MYC	Oncogenic Mutations	Uniq mutation in Liver metastasis	Berzosertib
ATM	Oncogenic SNV Mutations	Uniq mutation in Peritoneal metastasis	Olaparib; Talazoparib + Enzalutamide
FGFR2	Oncogenic Mutations, Amplification	Uniq mutation in Peritoneal metastasis	Erdafitinib; AZD4547; RLY-4008
BRCA1	Oncogenic Mutations	Uniq mutation in Peritoneal metastasis	Rucaparib
SMAD4	Oncogenic Mutations	Uniq mutation in Peritoneal metastasis	Capecitabine + Cetuximab + Gemcitabine + Oxaliplatin + Radiotherapy
ESR1	Oncogenic Mutations	Uniq mutation in Peritoneal metastasis	Letrozole + Taselisib; Fulvestrant + Pictilisib; Capivasertib + Paclitaxel
PIK3CA	Oncogenic SNV Mutations	Uniq mutation in Peritoneal metastasis	Alpelisib + Fulvestrant; RLY-2608; LOXO-783; Sirolimus; Everolimus

signatures corresponded to COSMIC_1 (spontaneous deamination of 5-methylcytosine) and COSMIC_3 (defects in DNA−DSB repair by HR) (Fig. 3G) [33]. In the PeM-MT group, the mutational signatures corresponded to COSMIC_1 (spontaneous deamination of 5-methylcytosine) (Fig. 3H). COSMIC_3 is linked to breast, ovarian, and pancreatic cancers. Platinum-responsive pancreatic cancer patients had COSMIC_3 signature mutations. No primary sample groups had the COSMIC_3 signature, although COSMIC_1 and COSMIC_6 (showing deficient DNA mismatch repair) was often seen (Supplementary Fig. S2). The findings suggested that the mutational characteristics of primary PDAC sites were similar across different metastatic sites, albeit with some variations observed among the latter.

3.4. Copy number variation (CNV) profile of paired samples

Pearson correlation analysis was utilized to investigate the congruity between the CNV profiles of paired primary and metastatic tumours. The distribution of the Pearson correlation coefficient was found to be irregular and discrete in both groups, as depicted Supplementary Figs. 3A–3B. This intriguing finding indicates that the copy number variation profile of the LiM-MT and PeM-MT cohorts exhibits significant intertumoral heterogeneity. The range of Pearson correlation coefficients was observed to be between −0.36 and 0.47 in LiM-Mts (Supplementary Fig. 3C). Additionally, a similar trend was observed in relation to PeM-Mts, indicating that the Pearson correlation coefficient ranged from −0.42 to 1 (Supplementary Fig. 3C). The statistical analysis demonstrated that the LiM group exhibited a comparable Pearson correlation coefficient to that of the PeM group ($p = 0.44$, Supplementary Fig. 3C).

3.5. Signaling pathway enrichment analysis between three primary foci or between paired samples

In order to determine whether somatic mutation landscapes influence cancer-related signalling pathways, we evaluated pathway-level enrichment. The KEGG database (https://www.kegg.jp) and gene set overrepresentation analysis on the segregated group were utilized to accomplish this. Enrichment analysis was performed on the genes impacted by somatic mutations in each of the four sample groups (LiM-PTs, LiM-MTs, PeM-PTs, and PeM-MTs) against each KEGG pathway. Similar to the SNV profile results, the pathway level exhibits several pathways that are specific to each group. Eleven GO terms were enriched in all samples, calmodulin binding and extracellular ligand-gated ion channel activity, and the other 2 terms were unique in the LiM-MT group compared to the PeM-MT group (Fig. 4A). In terms of KEGG enrichment analysis, 8 KEGG pathways were significantly enriched in these sample groups. LiM-PTs have a unique metastasis-related pathway, such as ECM-receptor interactions, which related to liver carcinoma development [34], were not enriched in the PeM group. Nevertheless, LiM-MTs have many more unique pathways other than LiM-PTs or PeM-MTs, such as proteoglycans in cancer, and the calcium signalling pathway is associated with tumour invasion (Fig. 4B) [35,36].

3.6. The subclonal architecture and phylogenetic relationships of paired primary and metastatic tumours

The process of clonal evolution, in which a clone that can metastasize is selected for dispersion to distant sites of secondary growth, is well known. High-resolution SNP profiling and mutation screening allowed us to determine the main and metastatic pairs' clonal and phylogenetic relationships. We used the VAF of variations to characterize the subclonal structures of paired tumour samples to study

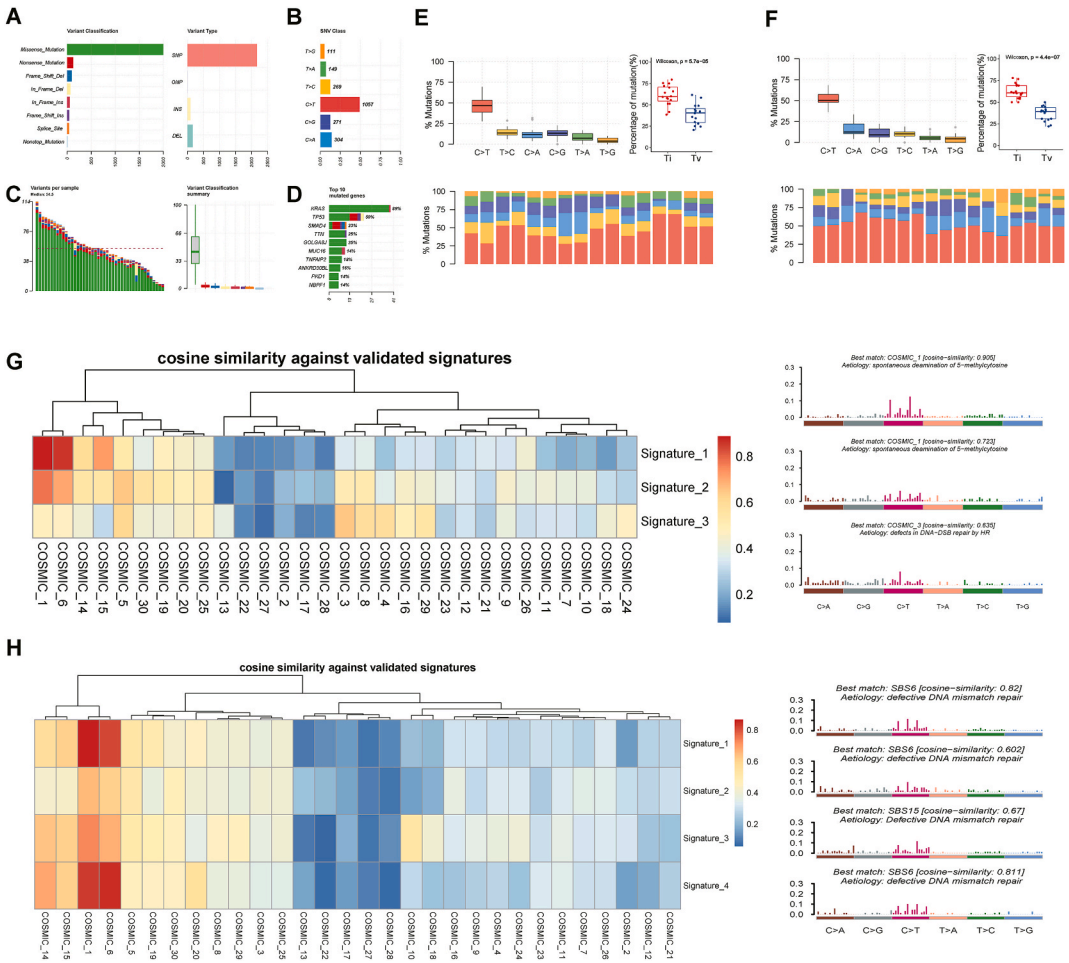

Fig. 3. A. Summary of mutation classification number in all 44 samples; B. The proportion of different SNV classifications in all 44 samples; C. The variants number per sample in all 44 samples; D. The top 10 mutated gene frequencies of all 44 samples; E-F. The ratio of base transformation to transversion was in the LiM group (E) and in the PeM group (F). G. The cosine similarity between the mutational signatures of the LiM-MT group and the validated COSMIC V2 signature (left panel). The identified mutational signatures of the LiM-MT group (right panel). H. The cosine similarity between the mutational signatures of the PeM-MT group and the validated COSMIC V2 signature (left panel). The identified mutational signatures of the PeM-MT group (right panel).

PDAC metastasis driving events. Furthermore, to elucidate the evolutionary routes of PDAC metastases, we examined all the phylogenetic trees of paired primary and metastatic tumours. The polygenic tree analysis revealed that the occurrence rate of *KRAS* trunk mutations in the peritoneal metastatic group was 77.8 % (7 out of 9), while in the liver metastasis group it was 87.5 % (7 out of 8). Similarly, the frequency of *TP53* trunk mutations in the two groups was 55.6 % (5 out of 9) and 37.5 % (3 out of 8), respectively. which revealed that *KRAS* plays an important role in metastasis and can drive metastasis events regardless of liver or peritoneal metastasis (Fig. 5A–B). Statistical analysis revealed that the LiM group had a similar proportion of trunk mutations as the PeM group ($p = 0.563$). However, the LiM-M group had a higher proportion of branch mutations than the PeM-M group ($p = 0.043$) (Fig. 5C). Notably, when *KRAS* was a branch mutation (P12, P20) (Fig. 5A–B, Fig. 6A) or without *KRAS* mutation (P17) (Figs. 5A and 6C), the subclone-based evolution architecture revealed that every subclone was relatively independent of each other. Principal component analysis (PCA) of clones and dynamic subclone-based evolution architecture analysis showed tended to be parallel evolution, as shown in Fig. 6B and D. It has been proven that oncogenic *KRAS* can recruit an expansive transcriptional network through mutant p53 to drive pancreatic cancer metastasis [37]. Subclonal architecture results of other patients are shown in Supplementary Fig. S4.

4. Discussion

Pancreatic ductal adenocarcinoma (PDAC), the classical and the most common subtype of pancreatic cancer, represents increased incidence and mortality rates worldwide. The liver is a common site for the metastasis of PDAC. In addition, it is worth noting that a considerable number of patients suffer from peritoneal metastasis, a significant yet inadequately studied factor contributing to morbidity and mortality [38]. Although several studies [39,40] have demonstrated that these two types of patients vary in terms of

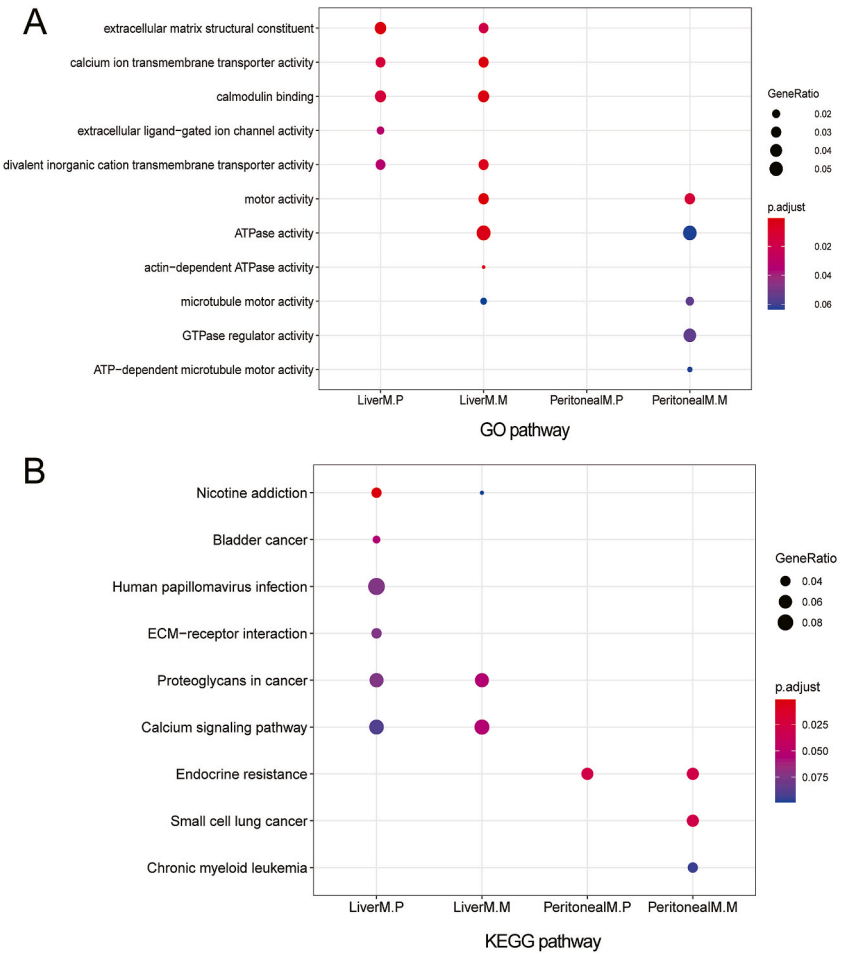

Fig. 4. A. GO enrichment analysis in primary-metastasis paired sample groups; B. KEGG enrichment analysis in primary-metastasis paired sample groups.

prognosis, both refer to a similar treatment now [41]. Nonetheless, the mechanisms that underlie the causes and prognostic disparities in metastases across various sites have yet to be elucidated. Thus, detailed research on PDAC metastatic site metastasis mechanisms is essential. In this study, we conducted WES on 44 samples obtained from 27 patients with PDAC. Our initial analysis focused on single nucleotide variants (SNVs) to elucidate the mutational landscape in two distinct metastatic groups: liver metastases and peritoneal metastases. The most observed alterations in our cohort were *KRAS* (89 %), *TP53* (50 %), *GOLGA8J* (25 %). These findings are further corroborated by prior research investigation [42]. Additionally, we noted a 50 % mutation frequency in *TP53* which was reported related to pancreatic cancer invasion and differentiation and has been reported to have a poorer prognosis than wild-type [43]. We examined how the genetic differences between liver and peritoneal metastases might inform the development of site-specific treatment strategies. In contrast to liver metastasis, peritoneal metastasis has mutations in DNA repair pathway genes such as *ATM* and *BRAC1*. At present, olaparib is FDA-approved for *BRCA1/2* mutant metastatic PDAC maintenance [44]. Our results revealed PDAC with peritoneal metastases may be an advantageous group for this treatment. The TMB is a powerful genetic biomarker that predicts immunotherapy success in several cancers. PeM-MTs had a lower TMB than LiM-MTs. This suggests immunotherapy may be a more effective treatment for liver metastases. A phase 1b/2 study evaluated surufatinib, camrelizumab, nab-paclitaxel, and S-1 (NASCA) as a first-line treatment for metastatic pancreatic cancer. The ORR for patients with liver metastases who received NASCA was significantly higher than that of those who did not (90.0 % vs. 20.0 %, $p = 0.0017$) [45]. However, the matched sample mutation landscape analysis showed that LiM- and PeM-metastatic tumours were consistent with their primary sites. CNV was not directly related to LiM or PeM when we examined the CNV pattern. The somatic and CNV alteration consistency between the primary and metastasis sites in the Li-M group exhibited similarities to the PDAC liver metastasis cohort recently reported by Sun et al. [42]. Additionally, Christine et al. [46] noted limited variability in driver gene mutations within primary and metastatic pancreatic cancer.

To further differentiate between LiM and PeM, we performed a comparative analysis of molecular pathways. Our results indicated enhanced activity in Gene Ontology (GO) pathways in LiM compared to PeM. Additionally, we identified distinct patterns of calmodulin binding between the two metastatic groups, suggesting site-specific molecular mechanisms underlying metastasis. The Ca++/calmodulin-dependent kinase superfamily categorises PKD [47]. According to Storz's findings [48], PKD1 has been implicated

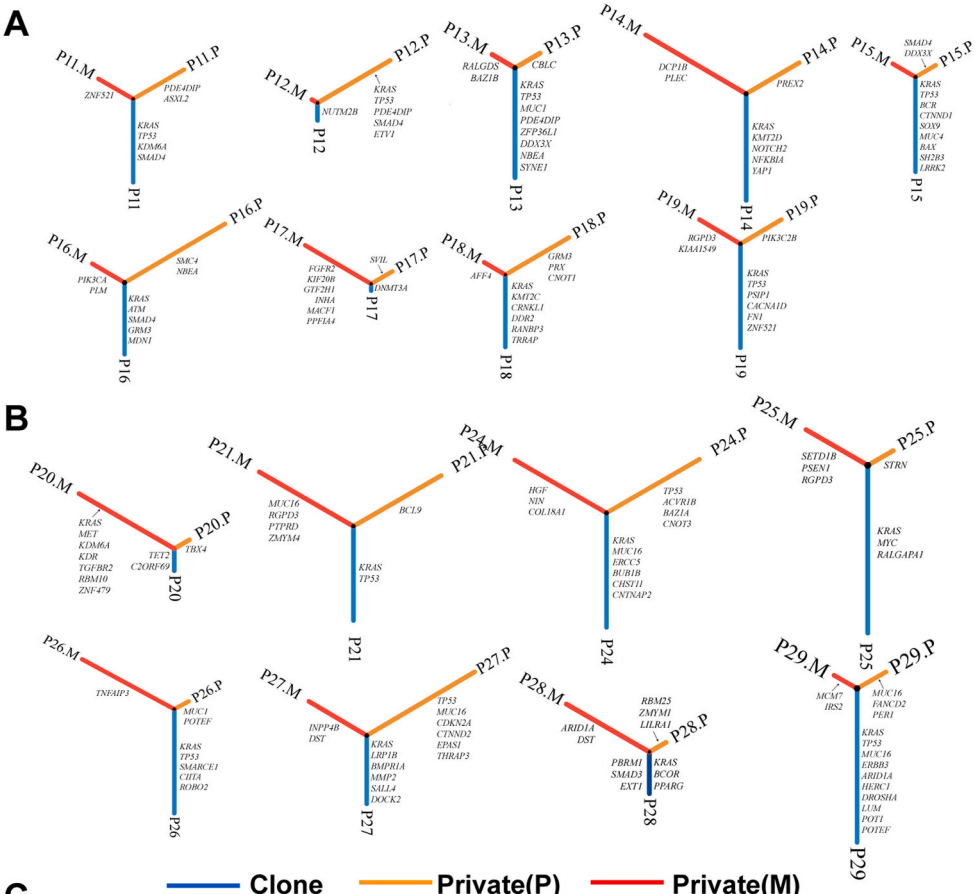

(caption on next page)

Fig. 5. Phylogenetic Analysis of Paired Primary Tumours and Metastases. Phylogenetic tree with the key variants highlighted in the PeM group (A) and LiM group (B), The phylogenetic trees illustrate the genetic relationships between primary pancreatic tumours and their corresponding metastases. Key genetic variants are highlighted to elucidate the evolutionary trajectories. In both trees, branch lengths represent the prevalence of shared genetic alterations or site-specific mutations in primary tumours or metastases. This visualization reveals distinct evolutionary patterns in organ-specific metastases. C. Statistical comparison of the proportions of private in primary or metastasis lesion and trunk mutations in the PeM group and LiM group.

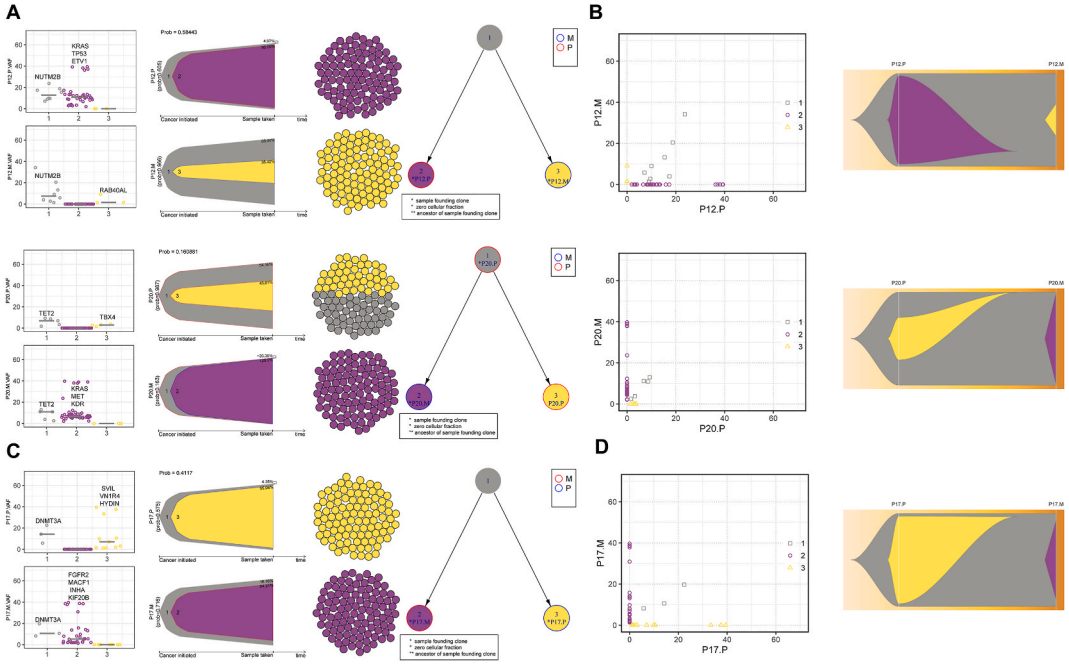

Fig. 6. Patterns of clonal evolution in the P12, P20 with KRAS branch mutation and P17 without KRAS branch mutation. A. Four components of the subclone-based evolution architecture in P12 and P20 From the left to the right, 1. Jitter plot of variant clusters, 2. Bell plots of clonal evolution in individual samples that are annotated with driver events. The probability of the various clones is annotated on the right end, which also indicates the time of sample collection. 3. A sphere of cells that represents the admixture of clones in individual samples, 4. Clonal evolution trees based on nodes that are annotated with samples that contain clones in primary or metastases; B. PCA analysis of different clusters in P12 and P20 (left panel), original model visualized using a fishplot whose width represents CCF of the clones in samples P12 and P20 (right panel); C. subclone-based evolution architecture in sample P17; D. PCA analysis of different clusters in P17 (left panel), original model visualized using a fishplot whose width represents CCF of the clones in samples P17 (right panel).

in the pathogenesis of pancreatic ductal adenocarcinoma, leading to the emergence of pancreatic intraepithelial neoplasia (PanIN). Furthermore, KEGG pathway analysis revealed that the LiM group exhibited distinct characteristics in terms of proteoglycans in cancer and the calcium signalling pathway. Juan et al. [49] discovered that Hyaluronan and proteoglycan link protein-1 in the extracellular matrix increase cancer cell malleability and pancreatic ductal adenocarcinoma metastasis. Numerous studies show that the calcium pathway affects pancreatic cancer progression and metastasis [36,50,51].

KRAS plays a crucial role in the biology of pancreatic cancer, and significant endeavors are currently being made to target this oncoprotein specifically [37]. *KRAS* mutations are the most common driver gene of PDAC, observed in up to 90 % of cases. Stepwise PDAC carcinogenesis is the most widely accepted model [52]. Firstly, *KRAS* mutations cause low-grade dysplastic pancreatic intraepithelial neoplasias (PanINs). Second, *TP53*, *CDKN2A*, *and SMAD4* mutations generally cause high-grade PanINs and invasive adenocarcinomas. The factors that drive and influence metastasis of pancreatic cancer remain a subject of ongoing debate. Then, we concluded by examining the evolution of clones in different metastases. The principal trunk mutations identified in both peritoneal and hepatic metastatic cohorts were *KRAS* and *TP53*. In general, *KRAS* branch mutations and the absence of mutations follow the progression model. This may be related to the manner in which *KRAS* promotes the metastasis of pancreatic cancer [53]. Nevertheless, it is worth noting that not all metastases within our cohort exhibited *KRAS* (PeM-MT vs. LiM-MT: 77.8 % (7/9) vs. 87.5 % (7/8)) or *TP53* mutations (PeM-MT vs. LiM-MT: 44.4 % (4/9) vs. 37.5 % (3/8)). Consequently, it can be inferred that *KRAS* mutations play a significant role in the spread of pancreatic cancer, while mutations in genes like *TP53* may also serve as potential stimulants.

Our study has several limitations that warrant consideration. The small sample size limited our ability to establish statistical significance for the high-frequency mutations observed in different metastatic sites. Additionally, the complexity of tumor metastasis requires more sophisticated analytical approaches.Future research should aim to increase sample sizes to improve statistical power and validate our findings, while also implementing comprehensive multi-omics analyses to capture the temporal and spatial heterogeneity

of pancreatic ductal adenocarcinoma (PDAC) metastasis. These advancements will deepen our understanding of the metastatic process in PDAC, potentially inform strategies to mitigate its progression, and enhance the clinical relevance of our findings, ultimately contributing to improved patient outcomes.

5. Conclusions

In conclusion, our study revealed that PeM and LiM exhibit not only a comparable somatic mutation landscape but also a similar evolutionary pattern at the genomic level. PeM-MTs are observed unique actionable mutations, including *ATM* and *BRCA1*. Additionally, liver metastases exhibit a higher TMB compared to peritoneal metastases. These findings provide evidence for the potential effectiveness of immunotherapy in treating liver metastases. These findings will offer fresh insights into the mechanism underlying different PDAC metastasis's location, as well as implications for more precisely treat specific distant metastases.

Ethics approval and consent to participate

The study protocol and all amendments were approved by the Institutional Review Boards of all participating institutions (Ethical number: 2021-03-B032). All participants provided written informed consent. The study was done in accordance with Good Clinical Practice guidelines and the Declaration of Helsinki.

Consent for publication

Not applicable.

Data availability

Has data associated with your study been deposited into a publicly available repository ?
No, data included in article/supp. material/referenced in article.

Funding

This study was supported by National Natural Science Foundation of China (82072692) and the Henan Provincial Health Commission (LHGJ20230445)

CRediT authorship contribution statement

Guoliang Yao: Writing – original draft, Formal analysis, Data curation. **Yanfeng Zhu:** Writing – original draft, Validation. **Chunhui Liu:** Supervision, Methodology. **Yanwen Man:** Writing – original draft, Conceptualization. **Kefeng Liu:** Supervision, Project administration. **Qin Zhang:** Writing – original draft, Visualization, Methodology, Formal analysis, Data curation. **Yuan Tan:** Writing – original draft, Investigation. **Qianqian Duan:** Writing – original draft, Investigation, Formal analysis, Data curation. **Dongsheng Chen:** Writing – review & editing, Validation. **Zunguo Du:** Writing – review & editing, Supervision, Conceptualization. **Yonggang Fan:** Writing – original draft, Visualization, Investigation, Formal analysis, Data curation.

Declaration of competing interest

The authors declare that they have no known competing financial interests or personal relationships that could have appeared to influence the work reported in this paper.

Acknowledgements

We thank Dr. Chuang Qi, Dr. Wanglong Deng, Dr. Guanghua Lu, Mrs. Liying Zheng, Miss. Junxiao Yan and Mr. Ran Ding from Jiangsu Simcere Diagnostics for their kind assistance.

List of abbreviations

Pancreatic ductal adenocarcinoma (PDAC)
Whole exome sequencing (WES)
liver metastases (LiM)
peritoneum metastases (PeM)
primary samples without metastasis (n; on-PTs)
unpaired samples (unpaired-PM)
tumour mutational burden (TMB)
primary tumours (PTs)

liver metastases (Li-M)
peritoneum Metastasis (Pe-M)
Integrated DNA Technologies (IDT)
formalin-fixed and paraffin-embedded (FFPE)
Jaccard similarity index (JSI)
variant allele frequency (VAF)
Kyoto Encyclopedia of Genes and Genomes (KEGG);
liver-metastatic primary lesions (LiM-PTs)
liver metastatic lesions (LiM-MTs)
peritoneal-metastatic primary lesions (PeM-PTs);
peritoneal metastatic lesions (PeM-MTs)
Single nucleotide polymorphisms (SNPs);
single nucleotide variants (SNVs)
Protein Kinase D (PKD);

Appendix A. Supplementary data

Supplementary data to this article can be found online at https://doi.org/10.1016/j.heliyon.2024.e35428.

References

[1] L.D. Wood, M.I. Canto, E.M. Jaffee, D.M. Simeone, Pancreatic cancer: pathogenesis, screening, diagnosis, and treatment, Gastroenterology 163 (2) (2022) 386–402.e1, https://doi.org/10.1053/j.gastro.2022.03.056.
[2] R.L. Siegel, K.D. Miller, H.E. Fuchs, A. Jemal, Cancer statistics, 2022, CA A Cancer J. Clin. 72 (1) (2022) 7–33, https://doi.org/10.3322/caac.21708.
[3] K.Y. Paik, S.H. Choi, J.S. Heo, D.W. Choi, Analysis of liver metastasis after resection for pancreatic ductal adenocarcinoma, World J. Gastrointest. Oncol. 4 (5) (2012) 109–114, https://doi.org/10.4251/wjgo.v4.i5.109.
[4] I. Thomassen, V.E. Lemmens, S.W. Nienhuijs, et al., Incidence, prognosis, and possible treatment strategies of peritoneal carcinomatosis of pancreatic origin: a population-based study, Pancreas 42 (1) (2013) 72–75, https://doi.org/10.1097/MPA.0b013e31825abf8c.
[5] L.R. Avula, B. Hagerty, C. Alewine, Molecular mediators of peritoneal metastasis in pancreatic cancer, Cancer Metastasis Rev. 39 (4) (2020) 1223–1243, https://doi.org/10.1007/s10555-020-09924-4.
[6] A. Moore, T. Donahue, Pancreatic cancer, JAMA 322 (14) (2019) 1426, https://doi.org/10.1001/jama.2019.14699.
[7] S. Valastyan, R.A. Weinberg, Tumor metastasis: molecular insights and evolving paradigms, Cell 147 (2) (2011) 275–292, https://doi.org/10.1016/j.cell.2011.09.024.
[8] T. Jiang, Z. Fang, S. Tang, et al., Mutational landscape and evolutionary pattern of liver and brain metastasis in lung adenocarcinoma, J. Thorac. Oncol. : official publication of the International Association for the Study of Lung Cancer 16 (2) (2021) 237–249, https://doi.org/10.1016/j.jtho.2020.10.128.
[9] J. Shi, X. Hua, B. Zhu, et al., Somatic genomics and clinical features of lung adenocarcinoma: a retrospective study, PLoS Med. 13 (12) (2016) e1002162, https://doi.org/10.1371/journal.pmed.1002162.
[10] S. Chen, Y. Zhou, Y. Chen, J. Gu, fastp: an ultra-fast all-in-one FASTQ preprocessor, Bioinformatics 34 (17) (2018) i884–i890, https://doi.org/10.1093/bioinformatics/bty560.
[11] H. Li, R. Durbin, Fast and accurate short read alignment with Burrows-Wheeler transform, Bioinformatics 25 (14) (2009) 1754–1760, https://doi.org/10.1093/bioinformatics/btp324.
[12] K. Cibulskis, M.S. Lawrence, S.L. Carter, et al., Sensitive detection of somatic point mutations in impure and heterogeneous cancer samples, Nat. Biotechnol. 31 (3) (2013) 213–219, https://doi.org/10.1038/nbt.2514.
[13] K. Wang, M. Li, H. Hakonarson, ANNOVAR: functional annotation of genetic variants from high-throughput sequencing data, Nucleic Acids Res. 38 (16) (2010) e164, https://doi.org/10.1093/nar/gkq603.
[14] J.T. Robinson, H. Thorvaldsdóttir, W. Winckler, et al., Integrative genomics viewer, Nat. Biotechnol. 29 (1) (2011) 24–26, https://doi.org/10.1038/nbt.1754.
[15] A. Fowler, S. Mahamdallie, E. Ruark, et al., Accurate clinical detection of exon copy number variants in a targeted NGS panel using DECoN, Wellcome open research 1 (2016) 20, https://doi.org/10.12688/wellcomeopenres.10069.1.
[16] Z. Hu, Z. Li, Z. Ma, C. Curtis, Multi-cancer analysis of clonality and the timing of systemic spread in paired primary tumors and metastases, Nat. Genet. 52 (7) (2020) 701–708, https://doi.org/10.1038/s41588-020-0628-z.
[17] A. Mayakonda, D.C. Lin, Y. Assenov, C. Plass, H.P. Koeffler, Maftools: efficient and comprehensive analysis of somatic variants in cancer, Genome Res. 28 (11) (2018) 1747–1756, https://doi.org/10.1101/gr.239244.118.
[18] S.A. Forbes, D. Beare, P. Gunasekaran, et al., COSMIC: exploring the world's knowledge of somatic mutations in human cancer, Nucleic Acids Res. 43 (Database issue) (2015) D805–D811, https://doi.org/10.1093/nar/gku1075.
[19] B. Vogelstein, N. Papadopoulos, V.E. Velculescu, et al., Cancer genome landscapes, Science (New York, NY) 339 (6127) (2013) 1546–1558, https://doi.org/10.1126/science.1235122.
[20] C. Kandoth, M.D. McLellan, F. Vandin, et al., Mutational landscape and significance across 12 major cancer types, Nature 502 (7471) (2013) 333–339, https://doi.org/10.1038/nature12634.
[21] D. Tamborero, A. Gonzalez-Perez, C. Perez-Llamas, et al., Comprehensive identification of mutational cancer driver genes across 12 tumor types, Sci. Rep. 3 (2013) 2650, https://doi.org/10.1038/srep02650.
[22] P. Kumar, S. Henikoff, P.C. Ng, Predicting the effects of coding non-synonymous variants on protein function using the SIFT algorithm, Nat. Protoc. 4 (7) (2009) 1073–1081, https://doi.org/10.1038/nprot.2009.86.
[23] R. Vaser, S. Adusumalli, S.N. Leng, M. Sikic, P.C. Ng, SIFT missense predictions for genomes, Nat. Protoc. 11 (1) (2016) 1–9, https://doi.org/10.1038/nprot.2015.123.
[24] I. Adzhubei, D.M. Jordan, S.R. Sunyaev, Predicting functional effect of human missense mutations using PolyPhen-2, Current protocols in human genetics (2013), https://doi.org/10.1002/0471142905.hg0720s76 **(Chapter 7)**:Unit7.20.
[25] H.A. Shihab, J. Gough, M. Mort, et al., Ranking non-synonymous single nucleotide polymorphisms based on disease concepts, Hum. Genom. 8 (1) (2014) 11, https://doi.org/10.1186/1479-7364-8-11.
[26] J.M. Schwarz, C. Rödelsperger, M. Schuelke, D. Seelow, MutationTaster evaluates disease-causing potential of sequence alterations, Nat. Methods 7 (8) (2010) 575–576, https://doi.org/10.1038/nmeth0810-575.

[27] C.A. Miller, B.S. White, N.D. Dees, et al., SciClone: inferring clonal architecture and tracking the spatial and temporal patterns of tumor evolution, PLoS Comput. Biol. 10 (8) (2014) e1003665, https://doi.org/10.1371/journal.pcbi.1003665.
[28] H.X. Dang, B.S. White, S.M. Foltz, et al., ClonEvol: clonal ordering and visualization in cancer sequencing, Ann. Oncol. : official journal of the European Society for Medical Oncology 28 (12) (2017) 3076–3082, https://doi.org/10.1093/annonc/mdx517.
[29] C.A. Miller, J. McMichael, H.X. Dang, et al., Visualizing tumor evolution with the fishplot package for R, BMC Genom. 17 (1) (2016) 880, https://doi.org/10.1186/s12864-016-3195-z.
[30] L.J. Revell, Ancestral character estimation under the threshold model from quantitative genetics, Evolution; international journal of organic evolution 68 (3) (2014) 743–759, https://doi.org/10.1111/evo.12300.
[31] I. Letunic, P. Bork, Interactive Tree of Life (iTOL) v5: an online tool for phylogenetic tree display and annotation, Nucleic Acids Res. 49 (W1) (2021) W293, https://doi.org/10.1093/nar/gkab301, w6.
[32] G. Yu, L.G. Wang, Y. Han, Q.Y. He, clusterProfiler: an R package for comparing biological themes among gene clusters, OMICS A J. Integr. Biol. 16 (5) (2012) 284–287, https://doi.org/10.1089/omi.2011.0118.
[33] A.J. Aguirre, J.A. Nowak, N.D. Camarda, et al., Real-time genomic characterization of advanced pancreatic cancer to enable precision medicine, Cancer Discov. 8 (9) (2018) 1096–1111, https://doi.org/10.1158/2159-8290.Cd-18-0275.
[34] Q.J. Zhang, D.Z. Li, B.Y. Lin, et al., SNHG16 promotes hepatocellular carcinoma development via activating ECM receptor interaction pathway, Hepatobiliary Pancreat. Dis. Int. : HBPD INT 21 (1) (2022) 41–49, https://doi.org/10.1016/j.hbpd.2021.09.006.
[35] J. Pan, N. Li, A. Renn, et al., GPC1-Targeted immunotoxins inhibit pancreatic tumor growth in mice via depletion of short-lived GPC1 and downregulation of wnt signaling, Mol. Cancer Therapeut. 21 (6) (2022) 960–973, https://doi.org/10.1158/1535-7163.Mct-21-0778.
[36] H.Y. Khan, G.B. Mpilla, R. Sexton, et al., Calcium release-activated calcium (CRAC) channel inhibition suppresses pancreatic ductal adenocarcinoma cell proliferation and patient-derived tumor growth, Cancers 12 (3) (2020), https://doi.org/10.3390/cancers12030750.
[37] M.P. Kim, X. Li, J. Deng, et al., Oncogenic KRAS recruits an expansive transcriptional network through mutant p53 to drive pancreatic cancer metastasis, Cancer Discov. 11 (8) (2021) 2094–2111, https://doi.org/10.1158/2159-8290.Cd-20-1228.
[38] Q. Li, X.X. Zhang, L.P. Hu, et al., Coadaptation fostered by the SLIT2-ROBO1 axis facilitates liver metastasis of pancreatic ductal adenocarcinoma, Nat. Commun. 14 (1) (2023) 861, https://doi.org/10.1038/s41467-023-36521-0.
[39] C. He, X. Huang, Y. Zhang, X. Lin, S. Li, The impact of different metastatic patterns on survival in patients with pancreatic cancer, Pancreatology : official journal of the International Association of Pancreatology (IAP) [et al] 21 (3) (2021) 556–563, https://doi.org/10.1016/j.pan.2021.01.014.
[40] H. Kolbeinsson, A. Hoppe, A. Bayat, et al., Recurrence patterns and postrecurrence survival after curative intent resection for pancreatic ductal adenocarcinoma, Surgery 169 (3) (2021) 649–654, https://doi.org/10.1016/j.surg.2020.06.042.
[41] S. De Dosso, A.R. Siebenhüner, T. Winder, et al., Treatment landscape of metastatic pancreatic cancer, Cancer Treat Rev. 96 (2021) 102180, https://doi.org/10.1016/j.ctrv.2021.102180.
[42] J. Yang, P. Lin, M. Yang, et al., Integrated genomic and transcriptomic analysis reveals unique characteristics of hepatic metastases and pro-metastatic role of complement C1q in pancreatic ductal adenocarcinoma, Genome biology 22 (1) (2021) 4, https://doi.org/10.1186/s13059-020-02222-w.
[43] Y. Zhou, J. Jin, Y. Ji, et al., TP53 missense mutation reveals gain-of-function properties in small-sized KRAS transformed pancreatic ductal adenocarcinoma, J. Transl. Med. 21 (1) (2023) 872, https://doi.org/10.1186/s12967-023-04742-y.
[44] T. Golan, P. Hammel, M. Reni, et al., Maintenance olaparib for germline BRCA-mutated metastatic pancreatic cancer, N. Engl. J. Med. 381 (4) (2019) 317–327, https://doi.org/10.1056/NEJMoa1903387.
[45] G.-H. Dai, R. Jia, H. Si, et al., A Phase 1b/2 Study of Surufatinib Plus Camrelizumab, Nab-Paclitaxel, and S-1 (NASCA) as First-Line Therapy for Metastatic Pancreatic Adenocarcinoma (mPDAC), American Society of Clinical Oncology, 2023.
[46] A.P. Makohon-Moore, M. Zhang, J.G. Reiter, et al., Limited heterogeneity of known driver gene mutations among the metastases of individual patients with pancreatic cancer, Nat. Genet. 49 (3) (2017) 358–366, https://doi.org/10.1038/ng.3764.
[47] A. Roy, J. Ye, F. Deng, Q.J. Wang, Protein kinase D signaling in cancer: a friend or foe? Biochim. Biophys. Acta Rev. Canc 1868 (1) (2017) 283–294, https://doi.org/10.1016/j.bbcan.2017.05.008.
[48] G.Y. Liou, H. Döppler, U.B. Braun, et al., Protein kinase D1 drives pancreatic acinar cell reprogramming and progression to intraepithelial neoplasia, Nat. Commun. 6 (2015) 6200, https://doi.org/10.1038/ncomms7200.
[49] L. Wiedmann, F. De Angelis Rigotti, N. Vaquero-Siguero, et al., HAPLN1 potentiates peritoneal metastasis in pancreatic cancer, Nat. Commun. 14 (1) (2023) 2353, https://doi.org/10.1038/s41467-023-38064-w.
[50] S.H. Jiang, L.L. Zhu, M. Zhang, et al., GABRP regulates chemokine signalling, macrophage recruitment and tumour progression in pancreatic cancer through tuning KCNN4-mediated Ca(2+) signalling in a GABA-independent manner, Gut 68 (11) (2019) 1994–2006, https://doi.org/10.1136/gutjnl-2018-317479.
[51] S. Arora, J. Tanwar, N. Sharma, S. Saurav, R.K. Motiani, Orai3 regulates pancreatic cancer metastasis by encoding a functional store operated calcium entry channel, Cancers 13 (23) (2021), https://doi.org/10.3390/cancers13235937.
[52] A.A. Connor, S. Gallinger, Pancreatic cancer evolution and heterogeneity: integrating omics and clinical data, Nat. Rev. Cancer 22 (3) (2022) 131–142, https://doi.org/10.1038/s41568-021-00418-1.
[53] X. Liu, W. Wang, X. Liu, et al., Multi-omics analysis of intra-tumoural and inter-tumoural heterogeneity in pancreatic ductal adenocarcinoma, Clin. Transl. Med. 12 (1) (2022) e670, https://doi.org/10.1002/ctm2.670.